RESEARCH PAPER

Green Synthesis and Characterization of Selenium Nanoparticles Using *Spirulina platensis* Extract and its Anticancer Activity Against SK-MEL-3 Skin Cancer Cells.

Jilsha G[1], Hemnath Elango[2*]

[1]Research Scholar, Faculty of Pharmacy, Karpagam Academy of Higher Education, Pollachi Main Road, Eachanari Post, Coimbatore- 641021, India.

[2*]Professor & Centre Head, Drug Testing Laboratory, Faculty of Pharmacy, Karpagam Academy of Higher Education, Pollachi Main Road, Eachanari Post, Coimbatore- 641021, India.

***Corresponding author: Hemnath Elango**

Professor & Centre Head, Drug Testing Laboratory, Faculty of Pharmacy, Karpagam Academy of Higher Education, Pollachi Main Road, Eachanari Post, Coimbatore- 641021, India.

*Email: hemnathelango@kahedu.edu.in

ABSTRACT

This study investigates the green synthesis of selenium nanoparticles (SP-S-NPs) using *Spirulina platensis* extract and evaluates their biological applications. SP-S-NPs were synthesised by combining *S. platensis* extract with selenium and ascorbic acid. Characterisation was performed using UV-visible spectroscopy, FT-IR, zeta size and potential analysis, X-ray diffraction, EDAX, FE-SEM and HR-TEM. SP-S-NPs conducted *in-vitro* anticancer activity against SK-MEL-3 skin cancer cells. SK-MEL-3 cells treated with SP-S-NPs (15 and 20 µg/ml) for 24 hours underwent apoptosis, as revealed by AO/EB staining. Fluorescence microscopy showed green live cells, yellow early apoptotic cells, and orange late apoptotic cells. Flow cytometry with Annexin V-FITC further confirmed apoptosis induction. UV-visible spectroscopy revealed surface plasmon resonance peaks at 340 nm, 400 nm, and 679 nm, confirming nanoparticle formation. FT-IR analysis identified various functional groups, while zeta size analysis showed an average particle size of 99.66 nm with a zeta potential of -23.5 mV, indicating good colloidal stability. X-ray diffraction, FE-SEM, and HR-TEM confirmed the crystalline nature and spherical to oval morphology of SP-S-NPs, with sizes ranging from 16.71 nm to 34.85 nm. SP-S-NPs demonstrated significant anticancer activity against SK-MEL-3 skin cancer cells, with an IC_{50} of approximately 20 µg/mL. Treatment with 15 and 20 µg/ml SP-S-NPs for 24 hr induced apoptotic changes, as evidenced by AO/EB staining. Fluorescence microscopy revealed green live cells, early apoptotic cells that read yellow with fragmented nuclei, and late apoptotic cells that appeared orange with chromatin condensation. Flow cytometry using Annexin V-FITC further confirmed apoptosis induction by SP-S-NPs. These findings suggest that SP-S-NPs synthesized using *S. platensis* extract have potential applications in cancer therapy and as antioxidants, warranting further investigation into their mechanisms of action and possible *in vivo* applications.

Keywords: Green synthesis, Selenium nanoparticles, *Spirulina platensis*, Anticancer activity, Apoptosis induction, SK-MEL-3 cells.

How to cite this article: Jilsha G, Elango H, Green Synthesis and Characterization of Selenium Nanoparticles Using Spirulina platensis Extract and its Anticancer Activity Against SK-MEL-3 Skin Cancer Cells. Int J Drug Deliv Technol. 2026;16(4s): 552-562; DOI: 10.25258/ijddt.16.4s.65

1. Introduction

Selenium nanoparticles (SeNPs) have gained significant attention recently due to their excellent bioavailability and low toxicity [1]. The green synthesis of SeNPs using biological methods has emerged as a safe and eco-friendly alternative to traditional chemical synthesis techniques. Among various biological sources, cyanobacteria, particularly Spirulina platensis, have shown great potential for producing SeNPs [2][3]. *S. platensis* is a blue-green microalga widely used in various industries due to its nutritional and medicinal properties. The ability of S. platensis to produce a wide variety of primary and secondary metabolites makes it an excellent candidate for reducing metal ions into nanoparticle form [4]. The biosynthesis of SeNPs using *S. platensis* involves the reduction of selenium ions to elemental selenium, forming stable nanoparticles. The synthesis process typically involves combining S. platensis extract with a selenium precursor, such as sodium selenite, under specific cultivation conditions. The reduction of selenium ions is visually indicated by a colour change in the medium from green to orange and finally to red. This colour change is a preliminary indicator of SeNP formation and can be quantitatively monitored using UV-visible spectroscopy. Several factors influence the synthesis and characteristics of SeNPs produced by *S. platensis*. The pH of the growth medium plays a crucial role in the formation and stability of the nanoparticles. Studies have shown that a neutral pH is optimal for SeNP synthesis using *S. platensis*. Additionally, the illumination schedule and cultivation time affect the size and polydispersity of the synthesised

*Author for Correspondence: hemnathelango@kahedu.edu.in

SeNPs. The characterisation of SeNPs produced by *S. platensis* involves various analytical techniques. Fourier-transform infrared spectroscopy (FT-IR) is used to identify the functional groups involved in the reduction and stabilisation of SeNPs [7]. X-ray diffraction (XRD) analysis confirms the crystalline nature of the nanoparticles. The size and morphology of the SeNPs are typically determined using techniques such as dynamic light scattering (DLS), scanning electron microscopy (SEM), and transmission electron microscopy (TEM). SeNPs synthesised using *S. platensis* extract have demonstrated promising biological activities. These nanoparticles exhibit significant antioxidant properties, often surpassing the antioxidant activity of sodium selenite. The antioxidant potential of SeNPs is evaluated using assays such as DPPH (2,2-diphenyl-1-picrylhydrazyl) and FRAP (ferric-reducing antioxidant power). SeNPs produced by S. platensis have shown potent antibacterial activity against various pathogenic bacteria [8][9]. This antibacterial action makes them potential candidates for developing new antimicrobial agents to combat drug-resistant bacterial strains. The green synthesis of SeNPs using *S. platensis* offers several advantages over traditional methods. It is a safe and environmentally friendly approach that eliminates the need for harsh chemicals and reduces the risk of generating toxic by-products. Additionally, the process is cost-effective and can be easily scaled up for large-scale production.

2. Material and methods

2.1. Collection and ethanolic extraction of S. *platensis*

S. platensis algae sample was collected from the National Facility for Marine Cyanobacteria (NFMC) at Bharathidasan University, Trichy, Tamil Nadu, India. Collected *S. platensis* was dried and stored in a cool place for further work. 500 grams of shade-dried *S. platensis* were crushed and placed in a filter paper thimble within chamber E of a Soxhlet apparatus. This apparatus, a standard extraction tool in chemistry, utilises heat to vaporise an ethanolic solvent from flask A [10]. The vapours condense in condenser D and drip onto the crude *S. platensis*, with ethanol chosen as the solvent for its ability to dissolve a wide range of phytochemicals. The extraction occurs through continuous contact between the plant material and the dripping extractant, ensuring thorough extraction of bioactive compounds. A siphon mechanism in tube C manages the liquid flow, recycling the solvent back to flask A when chamber E fills, enhancing extraction efficiency. The process continues until a drop from the siphon tube evaporates without residue, indicating complete extraction. The resulting crude ethanolic extract, now saturated with bioactive compounds, is preserved for further phytochemical examination (Figure 2).

Percentage of yield of ethanolic extract of *S. platensis*

The extraction efficiency of *S. platensis* is quantitatively assessed through percentage yield calculations that compare actual extract quantities against theoretical maximum extractable amounts. These calculations involve two primary methodologies: first, comparing the actual ethanolic extract yield to the theoretical yield by dividing the actual yield by the theoretical yield and multiplying by 100, and second, determining the dried crude extract yield by measuring the weight transformation from wet to lyophilised state. By dividing the dry crude extract weight by the wet crude extract weight and multiplying by 100, researchers can precisely evaluate extraction procedural efficiency, moisture content reduction, and biomass processing variations. These percentage yield measurements serve as critical analytical tools that provide comprehensive insights into the extraction dynamics, enabling systematic documentation of extract concentration, quality, and potential variations in the experimental process, ultimately supporting rigorous scientific investigation and methodology optimisation for *S. platensis* extract production [11].

Phytochemical evaluation of *S. platensis*

Ethanolic extracts of *S. platensis* were subjected to phytochemical screening using standard procedures, revealing the presence of various bioactive compounds. These compounds contribute to the algae's potential health benefits and applications in nutraceuticals.

LC-MS analysis of *S. platensis*

The chromatographic analysis shows three distinct HPLC profiles using 0.1% ammonium acetate in H_2O with 100% ACN as the mobile phase [12]. The separation was performed using specific gradient conditions (T/MB: 0/10, 1/10, 8/95, 10/95-10.5/10,14/10) with LCWLP-D M2MIX methodology for compound identification (Figure 2).

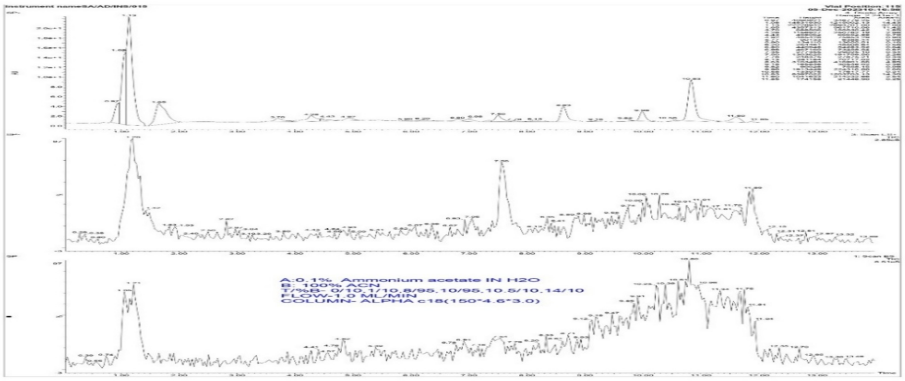

Figure 1: LC-MS analysis of the extract of *S. platensis*

Synthesis of Ethanolic extracts of *S. platensis* selenium nanoparticles

The synthesis of selenium nanoparticles was conducted through a carefully controlled process utilising *S. platensis* extract. The procedure involved combining 10 mL of the extract with 20 mL of 50 mM selenium solution using a magnetic stirrer for thorough mixing. The reduction reaction was initiated by adding 200 µL of 40 mM ascorbic acid. Two control conditions were established: a positive control of selenium mixed with 200 µL of 40 mM ascorbic acid for selenium nanoparticle synthesis and a negative control containing plant extract with 200 µL of 40 mM ascorbic acid. The resulting ruby red selenium nanoparticles were suspended in solution and subsequently centrifuged to obtain a powder form, which was then preserved for further analytical procedures.

Characterisation of *S. platensis* extract selenium nanoparticles (SP-S-NPs)

The morphological and structural characterisation of nanoparticles involved multiple analytical techniques. Initial morphological assessment was conducted using light microscopy and surface plasmon resonance measurements using a BioSpec Nano (Shimadzu). Functional group analysis was performed using ATR-FTIR spectrometry [3]. The crystalline structure was examined using an XPERT-PRO X-ray diffractometer, while detailed surface morphology and microscopic characteristics were analysed using FE-SEM (TESCAN) and HRTEM (JEOL) [9]. Particle size distribution and zeta potential measurements of liquid suspensions were determined using a Malvern Zetasizer Nano ZS, providing comprehensive data on particle stability and size characteristics.

Antioxidant activity

The antioxidant activity of SP-S-NPs was evaluated through a DPPH radical scavenging assay, with ascorbic acid serving as the standard reference. The analysis was conducted across 0 to 100 µg [13].

***In-vitro* skin cancer studies, MTT assay.**

Selenium nanoparticles (F1) cytotoxicity was evaluated using the MTT assay on SK-MEL-3 cells. The experimental procedure involved seeding cells at a concentration of 1×10^4 cells/ml in 96-well plates, followed by a 24-hour incubation period to ensure cell adherence. Subsequently, the cells were exposed to control, standard (STD), and F1 formulations and incubated for 24 hrs at 37°C in a humidified environment with 95% air and 5% CO_2. Post-incubation, the cells underwent a washing step, after which MTT dye (5 mg/mL in PBS) was introduced to each well. A 4-hour incubation period allowed the formation of purple formazan crystals, which were then solubilised using 100 µl of DMSO. The absorbance of the resulting solution was quantified at 540 nm using a multi-well plate reader. Cell viability was calculated as a percentage relative to the control group. The inhibitory concentration (IC_{50}) values, representing the concentration at which 50% cytotoxicity occurred, were determined from the dose-response curves. To ensure reliability, all experiments were performed in triplicate and repeated a minimum of three times.

AO/EB staining

SK-MEL-3 cells were cultured in 6-well plates at a density of 5×10^4 cells per well and allowed to adhere for 24 hours. The cells were then exposed to STD, F1, and Blank 1 treatments for an additional 24-hour period. Following treatment, the cells were harvested, rinsed with cold PBS, and subjected to a dual staining procedure using a 1:1 mixture of acridine orange (AO, 100 µg/ml) and ethidium bromide (EB, 100 µg/ml) at ambient temperature for 5 minutes. The stained cell samples were examined under a fluorescence microscope at 40x magnification. In a subsequent step, the treated cells were collected, washed thoroughly with PBS (three times), and re-stained using the same AO/EB mixture for 5 minutes. These samples were then immediately analysed under the fluorescence microscope at 40x magnification. The number of apoptotic cells was determined relative to the total cell count within the microscopic field of view to quantify the extent of apoptosis.

Annexin V apoptosis assay by flow cytometry method

The assessment of apoptosis was conducted using the ANNEXIN A5-FITC-Apoptosis Detection Kit from Beckman Coulter, adhering to the manufacturer's guidelines. The procedure involved resuspending cell pellets from the control group and the SP-S-NPs and SP-

S-NPs-treated groups in 1X binding buffer to achieve a 5×10^6 cells/ml concentration. Subsequently, each sample was supplemented with 1µL of annexin A5-FITC and 5µL of propidium iodide (PI). The prepared samples were then incubated on ice for 15 minutes. Following the incubation period, the samples were subjected to flow cytometric analysis to quantify the extent of apoptosis in the different treatment groups [16].

RESULTS AND DISCUSSION

Phytochemical analysis

The LC-MS analysis of *S. platensis* ethanolic extract revealed the presence of five significant bioactive compounds. α-Linolenic Acid (MW: 279) and Polyunsaturated Fatty Acids (MW: 279.1), both essential fatty acids, demonstrate the extract's potential nutritional value and anti-inflammatory properties. Tocopherol (MW: 430.71), a form of Vitamin E, indicates strong antioxidant capabilities that can protect cells from oxidative stress. Quercetin (MW: 302.2), a flavonoid known for its potent antioxidant and anti-inflammatory properties, further enhances the extract's therapeutic potential. The detection of Phenolic Acids (MW: 182.9) suggests additional antioxidant activity and potential antimicrobial properties. The diverse bioactive compounds identified in the extract suggest synergistic effects that could contribute to various biological activities. Combining antioxidants (Tocopherol, Quercetin, and Phenolic Acids) alongside essential fatty acids indicates that *S. platensis* extract could be a promising candidate for therapeutic applications, particularly in oxidative stress and inflammation conditions.

S. platensis ethanolic extracts selenium nanoparticles

The successful synthesis of selenium nanoparticles using *S. platensis* ethanolic extract was visually confirmed through distinct colour transitions. The process culminated in forming a characteristic reddish-brown colloidal solution, a changes indicator of selenium nanoparticle formation. This colour transformation from the initial extract to the final suspension demonstrates the effective reduction process. It validates the green synthesis approach for producing stable selenium nanoparticles using *S. platensis* extract as a reducing agent (Figure 1).

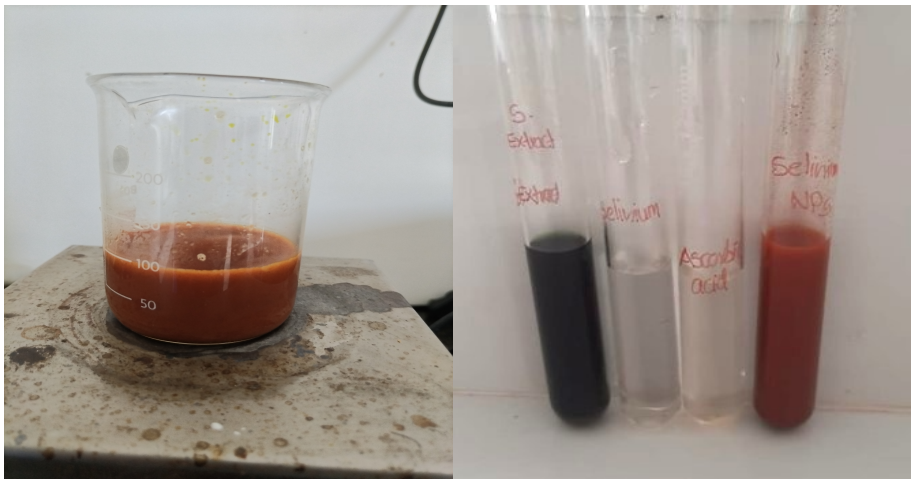

Figure 1: Synthesis of *S. platensis* extract and selenium nanoparticles.

Characterisation of SP-S-NPs

The UV-visible spectroscopic analysis of SP-S-NPs revealed distinctive surface plasmon resonance (SPR) characteristics across the 100-800 nm range (Figure 2). The spectra exhibited three prominent SPR peaks at 340 nm, 400 nm, and 679 nm, confirming successful nanoparticle synthesis. These multiple peaks suggest the presence of diverse nanoparticle morphologies correlating with the spherical and oval shapes previously observed through electron microscopy. The peak at 340 nm indicates the presence of smaller nanoparticles with high electron density, while peaks at 400 nm and 679 nm likely correspond to larger particles or those with distinct crystalline structures. The well-defined SPR bands validate the nano-scale formation and indicate stable particle dispersion with minimal aggregation, making these nanoparticles suitable for potential biomedical and catalytic applications.

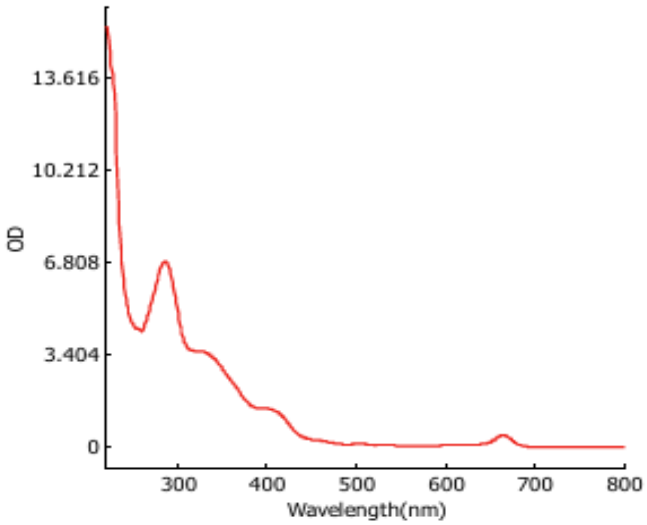

Figure 2: UV spectrum of SP-S-NPs.

FT-IR analysis of SP-S-NPs

The FTIR spectroscopic analysis of SP-S-NPs confirmed the successful reduction of CuSO4.5H2O by Spirulina platensis extract (Figure 3). The spectrum revealed characteristic peaks at 3341.15, 2151.66, 1638.23 and 559.33, 509.47, 544.46 cm-1, indicating O-H and N-H stretching of secondary amines. Additional peaks observed at 1638 cm-1 were attributed to C=O functional groups, validating the presence of key molecular interactions in the synthesised nanoparticles.

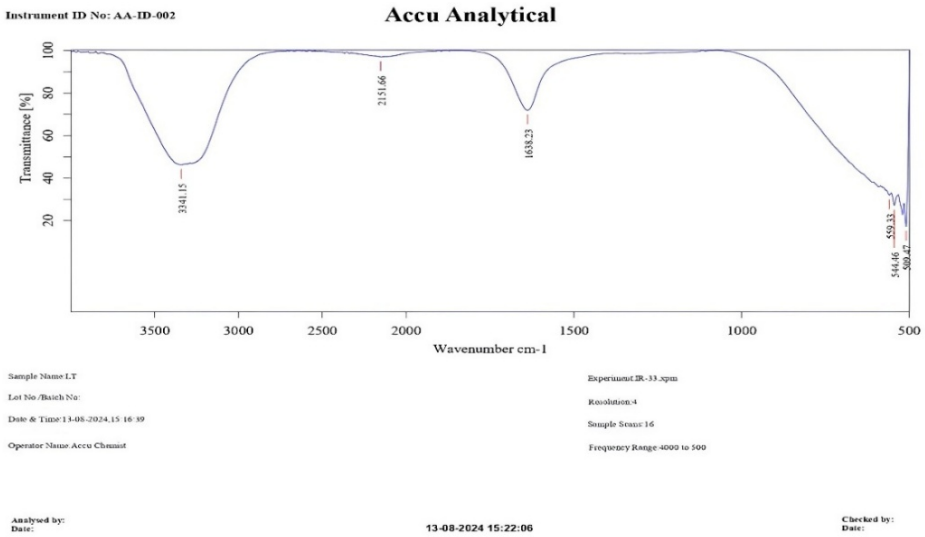

Figure 3: SP-S-NPs FT-IR spectrum.

SP-S-NPs Zeta Size and Potential Analysis

The dynamic light scattering analysis revealed that the synthesised SP-S-NPs exhibited an average particle size of 99.66 nm (Figure 4A), confirming their nanoscale dimensions and corroborating the electron microscopy observations. The zeta potential measurement indicated a value of -23.5 mV (Figure 4B), demonstrating favourable colloidal stability. This negative surface charge, exceeding the ±20 mV threshold typically associated with stable colloidal systems, suggests strong electrostatic repulsion between particles that effectively prevents aggregation in aqueous media. The significant negative zeta potential indicates the presence of surface-bound anionic groups, likely carboxylates or similarly charged species, which contribute to the particles' stability. These physicochemical characteristics - the optimal size distribution and robust surface charge - establish SP-S-NPs as stable nano formulations suitable for various biomedical applications, particularly in drug delivery and bioimaging, where consistent particle dispersion is crucial for maintaining therapeutic efficacy.

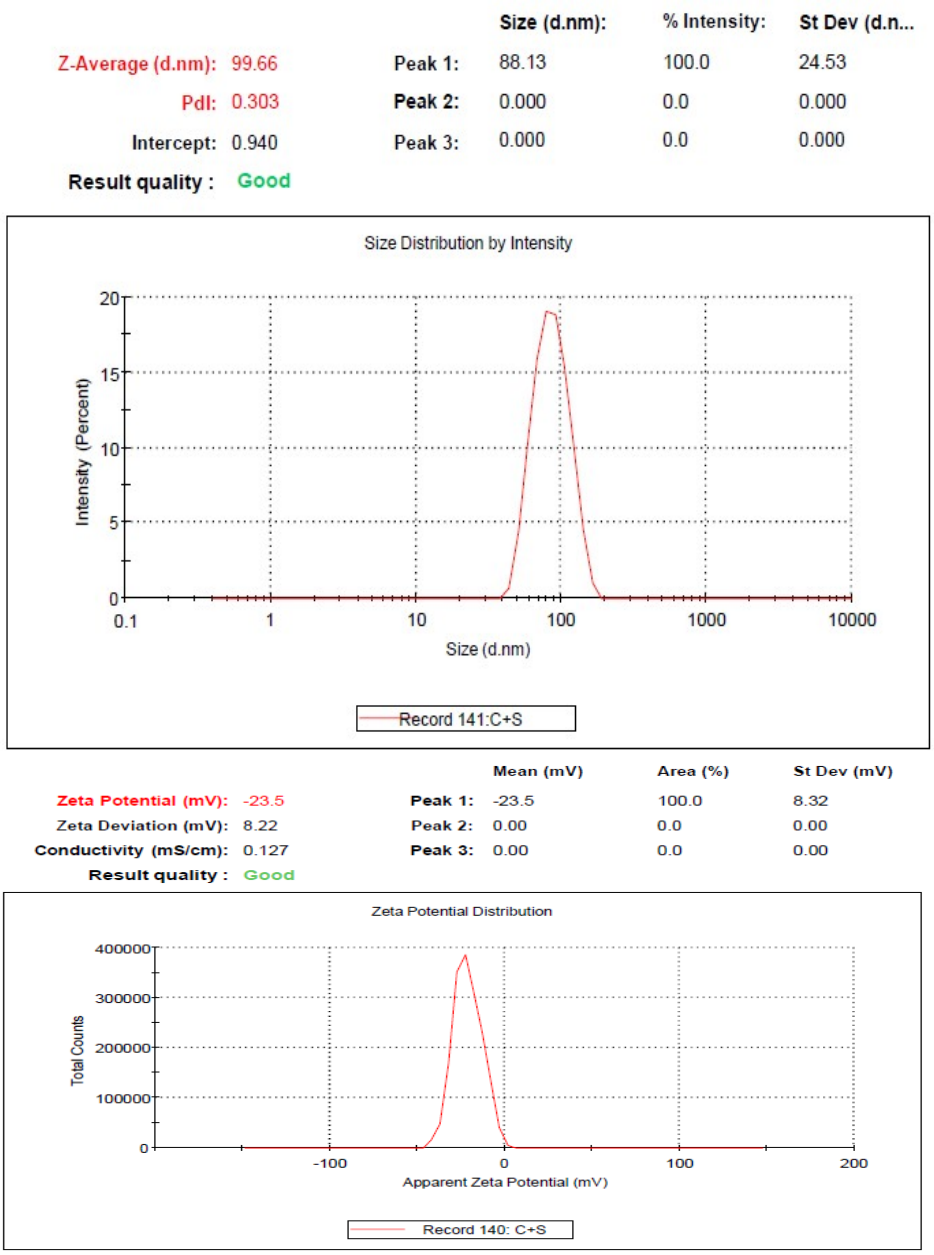

Figure 4: A: SP-S-NPs average zeta size 99.66 d. nm, B: SP-S-NPs zeta potential -23.5 mV.

X-RD analysis of SP-S-NPs

X-ray diffraction analysis of SP-S-NPs revealed a crystalline structure with a prominent peak at 2θ = 33.63°. This peak confirms the crystalline nature of the *S. platensis* extract nanoparticles and indicates a well-defined atomic arrangement within the particles (Figure 5).

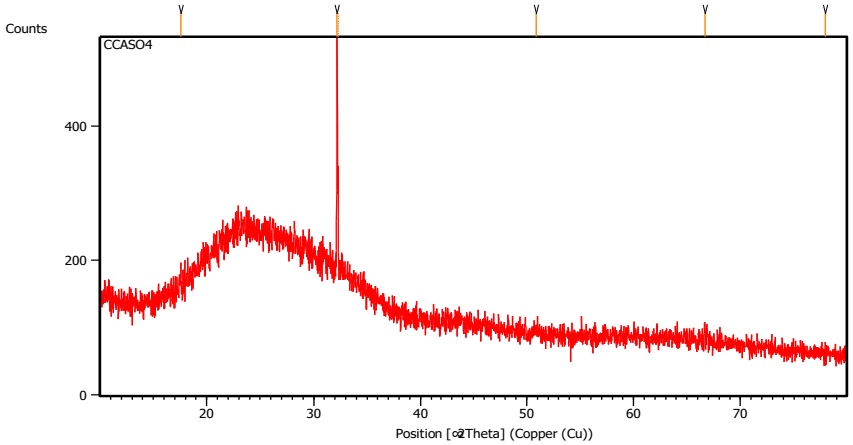

Figure 5: SP-S-NPs X-ray diffraction analysis.

EDAX analysis of the SP-S-NPs

EDAX spectroscopy provided insight into the elemental composition of SP-S-NPs, as illustrated in Figure 6. The analysis revealed the presence of selenium metal and carbon, hydrogen, and oxygen derived from the *S. platensis* extract. This composition reflects the nanoparticles' successful incorporation of metallic and organic components.

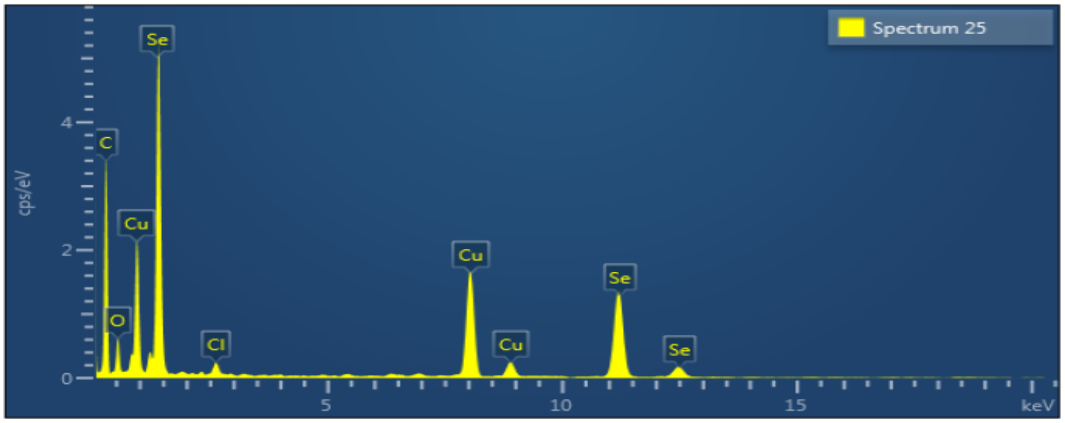

Figure 6: SP-S-NPs elements composition.

SP-S-NPs observation by electron microscope (FE-SEM and HRTEM).

Electron microscopy techniques, including FE-SEM and HR-TEM, provided conclusive evidence of SP-S-NPs' nano-scale dimensions and morphological characteristics. The particles exhibited both oval and spherical shapes, with size distribution analysis revealing a range of 16.71-34.85 nm (Figure 7). This size range is advantageous for biomedical applications, such as drug delivery, due to enhanced cellular uptake and tissue penetration capabilities. The predominant spherical shape of SP-S-NPs is beneficial, minimising surface area-to-volume ratio and thereby improving stability while reducing agglomeration in biological environments. The observed uniformity in particle size suggests a well-controlled synthesis process crucial for maintaining consistent physical and chemical properties. The size variation can be attributed to factors like synthesis conditions and surfactant concentration, which require careful optimisation for specific therapeutic applications.

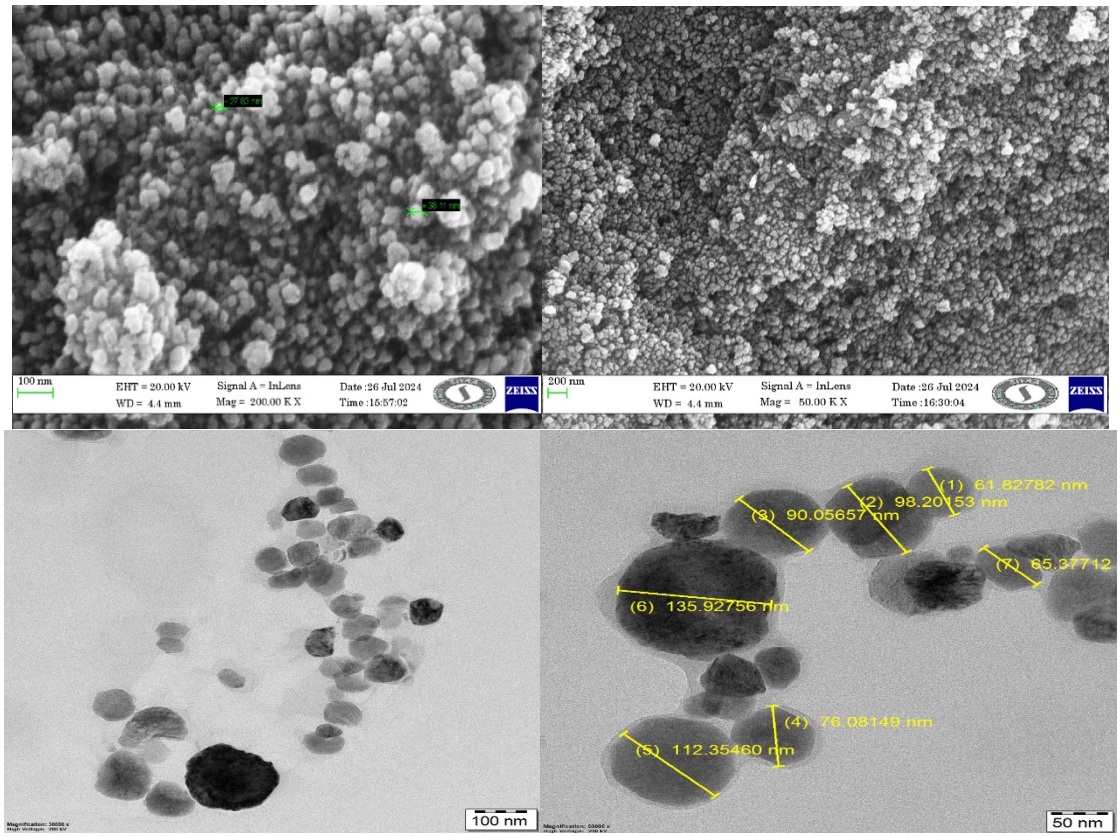

Figure 7: A: SP-S-NPs FE-SEM observation, B: SP-S-NPs HR-TEM observation.

Antioxidant activity of SP-S-NPs

The graph demonstrates the antioxidant activity of SP-S-NPs compared to ascorbic acid using a DPPH assay. While both compounds showed concentration-dependent inhibition, ascorbic acid exhibited higher antioxidant activity at lower concentrations (Figure 8). SP-S-NPs reached approximately 75% inhibition at 100 µg/mL, indicating significant antioxidant potential.

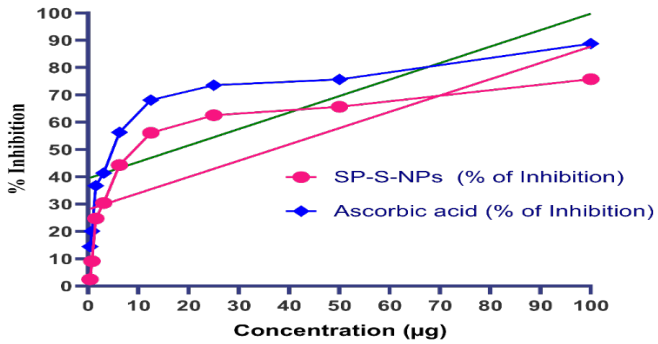

Figure 8: Antioxidant activity SP-S-NPs

Morphological changes in control and sample SP-S-NPs treated SK-MEL-3 cells for 24 h.

Figure 9 illustrates the morphological changes in SK-MEL-3 cells after 24-hour treatment with SP-S-NPs. Control cells displayed normal, intact morphology, while treated cells (15 and 20 µg/ml) exhibited clear signs of apoptosis (Figure 10). These signs included cell shrinkage, detachment from the surface, membrane blebbing, and distorted cellular shapes. The images, captured using a Bio-Rad fluorescent microscope, provide compelling evidence of the potential anticancer effects of SP-S-NPs on SK-MEL-3 melanoma cells. The observed dose-dependent changes suggest that higher concentrations of SP-S-NPs induce more pronounced apoptotic responses, highlighting their promising role in cancer treatment strategies (Figure 11).

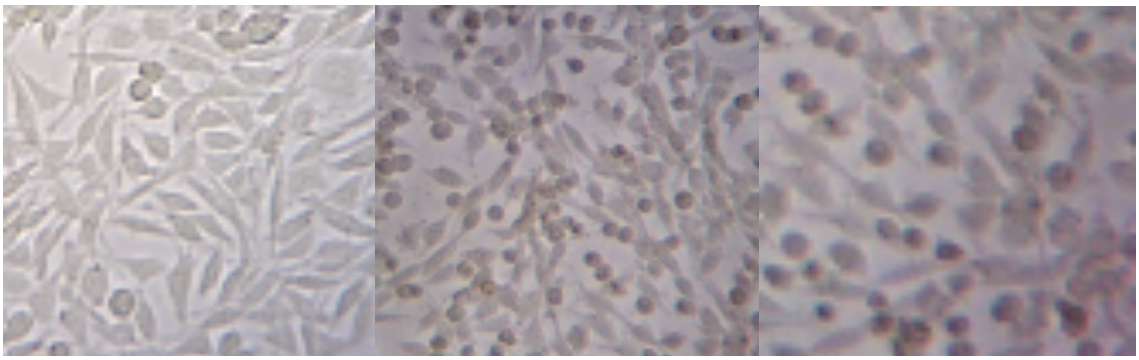

Control 15 µg/ml 20 µg/ml

Figure 9: Morphological changes in control and sample SP-S-NPs treated SK-MEL-3 cells for 24 h.

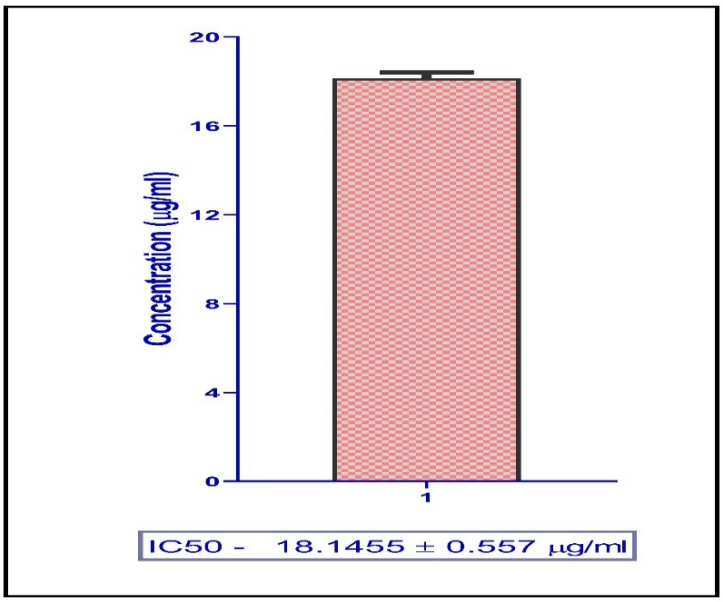

Figure 10: IC_{50} value SP-S-NPs.

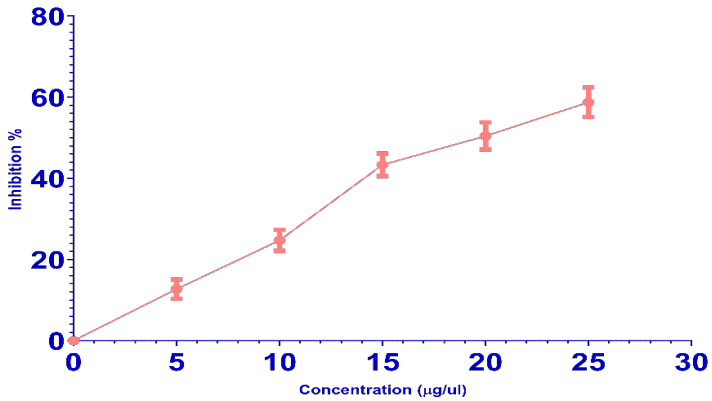

Figure 11: Percentage Inhibition of SK-MEL-3 cells.

AO/EB staining

The AO/EB staining revealed distinct morphological changes in SK-MEL-3 cells treated with STD and F1 compared to the control (Figure 12). Treated cells exhibited characteristic signs of apoptosis, including chromatin condensation, nuclear fragmentation, and membrane blebbing. The fluorescence microscopy images showed a higher proportion of orange-red apoptotic cells in the treated groups, indicating increased cell death compared to the predominantly green viable cells in the control group.

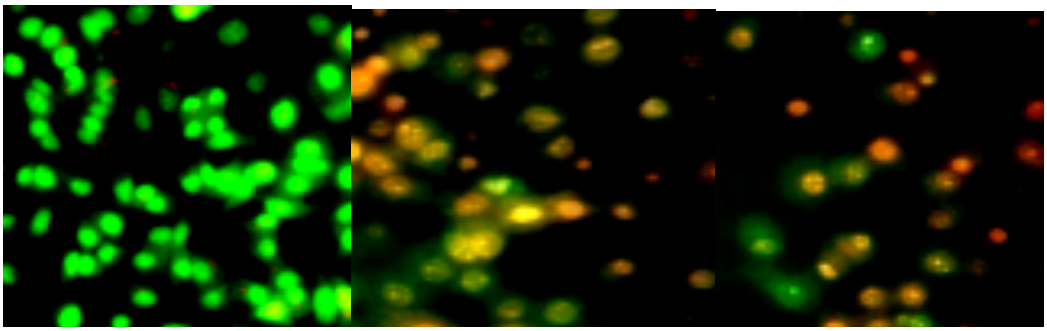

Control 15 µg/ml 20 µg/ml

Figure 12: Apoptotic staining – control & sample SP-S-NPs treated SK-MEL-3 cells for 24 h.

Annexin V apoptosis assay by the flow cytometry method

The flow cytometry analysis reveals distinct differences between control and SP-S-NP-treated samples (Figure 13). The control sample shows predominantly viable cells, with 97.26% in the lower left quadrant (Q4-LL), while only 1.46% and 1.22% of cells were in early and late apoptotic stages, respectively. In contrast, the SP-S-NPs-treated sample demonstrates significant apoptotic induction, with 53.54% of cells in late apoptosis (Q4-LR) and 7.36% in early apoptosis (Q4-UR). The treated sample also shows a reduced viable cell population (36.31% in Q4-LL), indicating the effective apoptosis-inducing properties of the SP-S-NPs treatment.

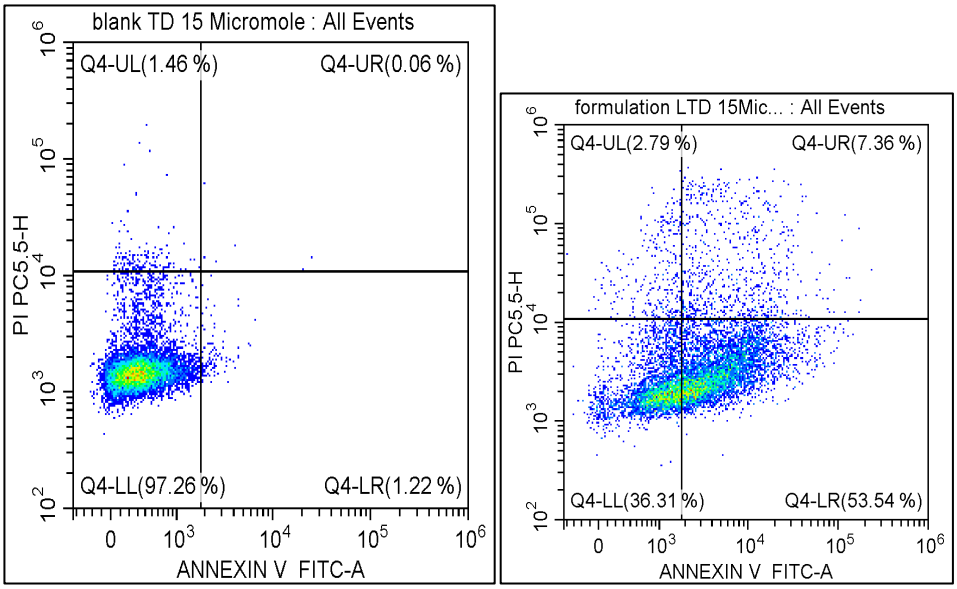

Control 20 µg/ml

Figure 13. flow cytometry analysis of SP-S-NPs-treated SK-MEL-3 cells

CONCLUSION

In conclusion, this study demonstrates the successful green synthesis and comprehensive characterisation of selenium nanoparticles using Spirulina platensis extract (SP-S-NPs). The nanoparticles exhibited optimal physicochemical properties, including crystalline structure, uniform morphology (16.71-34.85 nm), and stable colloidal dispersion (-23.5 mV zeta potential). LC-MS analysis revealed the presence of bioactive compounds such as α-Linolenic Acid, Tocopherol, and Quercetin, contributing to the extract's therapeutic potential. The SP-S-NPs demonstrated significant antioxidant activity, achieving 75% DPPH inhibition at 100 µg. Most notably, the nanoparticles showed promising anticancer effects against SK-MEL-3 melanoma cells, inducing pronounced apoptotic responses at 15 and 20 µg/ml concentrations. Flow cytometry analysis confirmed their efficacy, with treated samples showing 53.54% late apoptotic cells compared to 1.22% in controls. These findings suggest that SP-S-NPs represent a promising platform for biomedical applications, particularly in cancer therapeutics, due to their controlled synthesis, stability, and significant biological activities. The combination of antioxidant properties and selective cytotoxicity against cancer cells warrants further investigation for potential therapeutic development.

CONFLICT OF INTEREST: Nil
FUNDING: Nil
ACKNOWLEDGEMENT: We express our gratitude for providing facilities and support to carry out the work

at Drug testing laboratory, Karpagam Academy of Higher Education, Coimbatore and Sanjo College of Pharmaceutical Studies, Vellappara, Palakkad, Kerala.

DATA AVAILABILITY: Data generated while conducting the research are available to the corresponding author upon reasonable request.

ABBREVIATIONS

UV: Ultraviolet.
FT-IR: Fourier Transform Infrared Spectroscopy
FE-SEM: Field Emission Scanning Electron Microscopy.
HR-TEM: High-Resolution Transmission Electron Microscopy.
EDAX: Energy Dispersive X-ray Analysis.
DLS: Dynamic light scattering.
XRD: X-ray Diffraction.
LC-MS: Liquid Chromatography-Mass Spectrometry.
SP-S-NPs: Spirulina platensis Selenium Nanoparticles.
DPPH: 2,2-diphenyl-1-picrylhydrazyl.
AO/EB: Acridine Orange/Ethidium Bromide.
SPR: Surface Plasmon Resonance.
PBS: Phosphate Buffered Saline.
SK-MEL-3: Human Melanoma Cell Line.

REFERENCES

1. Zhang X, Yan H, Ma L, Zhang H, Ren DF. Preparation and characterization of selenium nanoparticles decorated by Spirulina platensis polysaccharide. *J Food Biochem*. 2020;44(9): e13363.
2. Alipour S, Kalari S, Morowvat MH, Sabahi Z, Dehshahri A. Green Synthesis of Selenium Nanoparticles by Cyanobacterium *Spirulina platensis* (abdf2224): Cultivation Condition Quality Controls. *Biomed Res Int*. 2021; 2021:6635297.
3. Alipour S, Kalari S, Morowvat MH, Sabahi Z, Dehshahri A. Green Synthesis of Selenium Nanoparticles by Cyanobacterium *Spirulina platensis* (abdf2224): Cultivation Condition Quality Controls. *Biomed Res Int*. 2021; 2021:6635297.
4. Mikhailova EO. Selenium Nanoparticles: Green Synthesis and Biomedical Application. *Molecules*. 2023;28(24):8125.
5. Sun K, Ma L, Hou J, et al. Physalis peruviana heteropolysaccharide-conjugated selenium nanoparticles: Preparation, characterization, and promising applications in cancer therapy. *Int J Biol Macromol*. Published online March 1, 2025. doi: 10.1016/j.ijbiomac.2025.141639.
6. Almessiere MA, Slimani Y, Korkmaz AD, et al. Magnetic Investigation of Se/In Codoped $Co_{0.5}Ni_{0.5}Fe_2O_4$ Spinel Nanoparticles Synthesized via the Sonochemical Route. *Inorg Chem*. Published online March 3, 2025. doi: 10.1021/acs.inorgchem.5c00276.
7. Li S, Yang H, Zhou W, et al. Selenium Nanoparticles Decorated With Stevioside Potentially Attenuate Fructose Palmitate Induced Lipid Accumulation in HepG2 Cells. *Mediators Inflamm*. 2025;2025:7942947.
8. Hashem AH, Salem SS. Green and ecofriendly biosynthesis of selenium nanoparticles using Urtica dioica (stinging nettle) leaf extract: Antimicrobial and anticancer activity. *Biotechnol J*. 2022;17(2):e2100432.
9. Bi Bi S, Elahi I, Sardar N, et al. Exploring non-cytotoxic, antioxidant, and anti-inflammatory properties of selenium nanoparticles synthesized from Gymnema sylvestre and Cinnamon cassia extracts for herbal nanomedicine. *Microb Pathog*. 2024;192:106670.
10. Shilpa V, Samuel Thavamani B, Roshni E, Sangeetha Vijayan U, Lekshmi M, Bhagyasree S, Jilsha G, Muddukrishnaiah K. Green synthesis Zinc Oxide nanoparticle using Allamanda cathartica leaf extract and their cytotoxic and antibacterial activity. nanomedicine research journal, 5 (3), 298-305. 2020.
11. Muddukrishnaiah, K., and Sumita Singh Sumita Singh. "Antimicrobial, synergistic activity and antioxidant studies on multidrug resistance human pathogen using crude extract of Azadirachta indica leaf and Withania somnifera rhizome." (2015): S3-009.
12. Yi X, Huang X, Xiong Y, Wu Y. A Highly Efficient and Automated Magnetic Bead Extraction Method Overcomes the Matrix Effect in LC-MS/MS Analysis of Human Serum Steroid Hormones. *J Am Soc Mass Spectrom*. Published online March 5, 2025. DOI:10.1021/jasms.4c00338.
13. Cruz LY, Wang D, Liu J. Biosynthesis of selenium nanoparticles, characterization and X-ray induced radiotherapy for the treatment of lung cancer with interstitial lung disease. *J Photochem Photobiol B*. 2019; 191:123-127.
14. Ezzat N, Emadeldien N, Ali MK, et al. In vitro Evaluation of Zinc Oxide-Metformin Folic Acid Nanocomposite as a Targeted Drug Delivery System for Cancer Therapy. *Asian Pac J Cancer Prev*. 2025;26(2):443-452.
15. Chi X, Feng L, Wang L, et al. Downregulation of lncRNA MNX1-AS1 promotes the ferroptosis and apoptosis of non-small cell lung cancer. *Int J Med Sci*. 2025;22(5):1052-1063.
16. Ahn CH, Myong JS, Ahmed KR, et al. A pharmacoinformatic approach for studying *Atractylodes Lancea* DC's anticancer potential and control ROS-mediated apoptosis against prostate cancer cells. *Front Oncol*. 2025; 15:1471110.